applied sciences

MDPI

Article

Protection of Buried Pipelines from High-Speed Train Vibrations with Expanded Polystyrene Geofoam

Alexandros Lyratzakis [1], Yiannis Tsompanakis [1,*] and Prodromos N. Psarropoulos [2]

[1] School of Chemical and Environmental Engineering, Technical University of Crete, 73100 Chania, Greece; alyratzakis@gmail.com
[2] School of Rural, Surveying and Geoinformatics Engineering, National Technical University of Athens, 15780 Athens, Greece; prod@central.ntua.gr
* Correspondence: jt@science.tuc.gr; Tel.: +30-28-2104-3194

Featured Application: The findings of this study can be applied in engineering practice for the protection of buried pipelines and other underground life lines crossing under or near continuously expanding high-speed railway lines.

Abstract: High-speed railway (HSR) lines commonly operate over hundreds of kilometers, crossing several other large-scale infrastructures, such as highways, tunnels, bridges, and pipelines. This fact makes adjacent infrastructure more vulnerable to high-speed train (HST)-induced vibrations; thus, their potential distress should be carefully examined. The current study aims to assess the level of traffic-induced vibrations on the surface of buried pipelines vertically crossing under an HSR line. Firstly, the necessity to reduce high vibration levels is highlighted, utilizing a three-dimensional (3D) finite element model in conjunction with the moving load approach. Subsequently, an efficient mitigation measure is proposed to minimize these vibrations. For this purpose, a low-weight, high-performance geosynthetic fill material, i.e., expanded polystyrene (EPS) geofoam blocks, has been implemented between the HSR line and the buried pipeline to minimize the impact of vibrations. In this manner, HST-induced vibrations are reflected on EPS blocks, preventing them from reaching the pipeline surface. Based on this detailed parametric study, useful conclusions are drawn regarding the mechanical properties and geometry of the EPS protection layer.

Keywords: high-speed railways; high-speed trains; train-induced vibrations; pipelines; mitigation measures; expanded polystyrene

check for updates

Citation: Lyratzakis, A.; Tsompanakis, Y.; Psarropoulos, P.N. Protection of Buried Pipelines from High-Speed Train Vibrations with Expanded Polystyrene Geofoam. *Appl. Sci.* **2024**, *14*, 1087. https://doi.org/10.3390/app14031087

Academic Editor: Krzysztof Zboiński

Received: 21 November 2023
Revised: 12 January 2024
Accepted: 18 January 2024
Published: 27 January 2024

Copyright: © 2024 by the authors. Licensee MDPI, Basel, Switzerland. This article is an open access article distributed under the terms and conditions of the Creative Commons Attribution (CC BY) license (https://creativecommons.org/licenses/by/4.0/).

1. Introduction

In recent years, train-induced vibrations and associated detrimental effects have become even more pronounced. The higher living standards of the population have increased the need for fast, safe, economical, and comfortable traveling. This fact has led to the development of new high-speed railway (HSR) lines and/or the upgrading of existing railways to become suitable for high-speed trains (HST) [1]. Hence, the impact of developed vibrations on the structural safety [2,3] and primarily the discomfort/disruption of residents' activities in adjacent buildings has become a crucial issue [4]. Train-induced vibrations are mainly propagated on the surface of the underlying soil in the form of surface Rayleigh waves. This complex phenomenon has drawn the attention of several researchers and engineers [5,6]. The growth of researchers' knowledge on numerical and analytical methodologies in recent years has contributed to the accurate prediction of the response of railway tracks and the subsoil's surface when subjected to HST-induced vibrations. Relevant investigations focus on wave propagation and surface vibrations [7] as well as on mitigation measures [8,9].

Vibrations due to HST passage can disturb the residents of adjacent buildings, affecting the railway lines and the safe operation of nearby infrastructure. In recent years, several studies have been performed to investigate these potential problems, including numerical approaches and field tests. In order to study this complex phenomenon, 2D, 2.5D, or 3D numerical boundary element—[8,10] or finite element [11,12]—based approaches have been used. The majority of the relevant studies have examined quite accurately the propagation of vibrations on the soil surface. Nonetheless, only a few studies have investigated the effects of developing vibrations induced by the passage of HSTs on the subsoil [13] and underground infrastructure [14].

Hence, in the present study, a first attempt is made to investigate the dynamic response of buried pipelines crossing an HSR line vertically, aiming to protect them using expanded polystyrene (EPS) blocks. EPS geofoam is a lightweight material widely used in various geotechnical applications [15,16]. The Norwegian Public Roads Administration (NPRA) introduced this low-cost, high-performance material as base layer in road construction in 1972 [17]. More specifically, the implementation of two layers of EPS blocks with a total height equal to 0.5 m resulted in a 5 kPa decrease in the weight surcharge. Since the first applications in transportation infrastructure, EPS has been widely used in many engineering projects worldwide to resolve various construction issues, including highways passing through sites of poor soils, road widening, lightweight rail embankments, bridge abutments fill, the protection of underground structures, and slope stabilization. For instance, Bartlett et al. [18] examined several techniques for protecting underground pipelines and culverts in transportation infrastructure by implementing EPS blocks.

In a recent work, Tafreshi et al. [19] presented a series of full-scale tests on underground pipelines subjected to traffic-induced loading and examined the reinforcement of these pipelines by implementing EPS geofoam and geocell as backfill layers. According to this study, the use of EPS blocks with a height equal to 0.3D and width 1.5D (where D is the pipe diameter) above the pipeline is proposed as a very practical and efficient mitigation measure. The beneficial role of the implementation of EPS backfills for the protection of buried pipelines subjected to other types of loading has also been investigated. Choo et al. [20] studied the beneficial role of EPS geofoam backfill for the protection of buried pipelines subjected to permanent ground displacements (e.g., surface faulting, land sliding, seismic settlement, and lateral spreading due to soil liquefaction). In the case of a strike-slip fault rupture, geofoam blocks decrease the axial tensile strain of a non-pressurized pipeline from 4.16% to 0.75% in the case of a crossing angle equal to 135° [21].

As previously mentioned, several studies have investigated the protection of underground pipes or culverts with the use of EPS geofoam [22,23]. Nevertheless, there is a lack of studies in the international literature focusing on the impact of railway traffic loads on buried pipelines. Thus, aiming to contribute to this research field, the present paper investigates the dynamic response of pipelines crossing vertically under HSR lines, thus being exposed to HST-induced vibrations as well as their protection with EPS blocks. Initially, the adopted numerical approach was compared with pre-existing experimented data. In the sequence, several types of pipes have been examined. Furthermore, the impact of the geofoam layer thickness, placed on the top of the pipeline, on the reduction in vibrations level has been investigated for three typical HST passing velocities. Apart from the level of vibrations, the reduction in the pipeline vertical diameter change, i.e., pipe ovalization, has also been examined as this can be detrimental for its integrity and safe operation. The findings of the conducted parametric study can be useful in engineering practice for the protection of buried pipelines, as well as other underground lifelines, crossing under or near continuously expanding HSR lines.

2. Materials and Methods

2.1. Validation of Numerical Methodology with Experimental Data for Polyethylene Pipelines and Road Moving Loads

As aforementioned, there are not any relevant bibliographic references with experimental data or in situ measurements investigating the distress of buried pipelines due to HST-induced vibrations. Nevertheless, there exist few experimental tests simulating the response of buried pipes due to traffic loads [19,24]. Tafreshi et al. [19] used a full-scale model to simulate the repeated loading of heavy traffic. More specifically, 14 tests were carried out using a high-density polyethylene pipe (HDPE 100) within unreinforced and reinforced soil with EPS geofoam blocks and geocells. The model was constructed on a test pit with a floor plan of 2.2 m $\times$ 2.2 m and a depth of 1 m. Furthermore, the test trench had dimensions of 0.75 m $\times$ 0.75 m and a 1.75 m depth. A circular plate repeatedly loaded/unloaded the test trench, aiming to simulate the traffic loads. The loading plate had a diameter of 250 mm; hence, a pressure equal to 800 kPa was applied in order to simulate the half axle of a heavy vehicle, while 150 loading cycles were imposed. Khalaj et al. [24] presented a similar full-scale model. The floor plan of the test pit was slightly smaller in this case, although the same pipe and a similar soil were used. Compared to the first test, a gradually increasing load had been placed on the plate in this case (instead of repeated traffic loads). More specifically, the load was increased linearly from 0 kPa to 800 kPa in 5 s.

In the present study, these two experimental investigations were used to validate a preliminary numerical model capable of accurately representing traffic loads. The material properties and dimensions of the tests have been simulated utilizing the commercial finite element (FE) software ABAQUS 6.14 [25] to provide a numerical model capable of predicting the response of a buried pipe when exposed to traffic-induced vibrations. Hexahedral linear elements with a reduced integration formulation (C3D8R), with size 50 mm, have been used to simulate the backfill trench and native soil. The pipeline has been modeled with linear four-node shell elements (S4R). Furthermore, the interaction between the loading plate and the soil surface has been assumed to be frictionless and "hard contact" conditions along the normal and tangential directions. Figure 1 illustrates the geometry of the employed FE model.

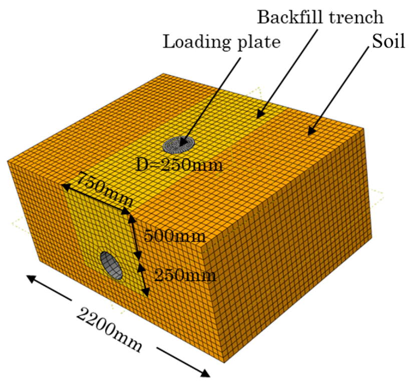

Figure 1. Three-dimensional FE model used for validation.

Initially, in the first analysis step, geostatic stress was imposed in the model. In the next step, pressure was applied on the rigid circular plate at the soil surface. In the sequence, pressure on the loading plate was applied in the second step to replicate the load pattern of the two pressure plate tests. More specifically, in order to simulate the repeated loading cycles of the model of Tafreshi et al. [19], a pressure equal to 800 kPa was applied 150 times on the pressure plate with a frequency of 0.33 Hz. In the second loading scenario, the pressure gradually increased from 0 kPa to 800 kPa, aiming to replicate the load of Khalaj et al.'s [24] experimental setup. Analysis was conducted based on the explicit dynamic module of ABAQUS, as it can achieve more accurate results in such dynamic problems with moving loads compared to the implicit dynamic module.

The mechanical properties of the HDPE100 pipe in both models were adopted from the study of Khalaj et al. [24]. The pipeline material has a density, Young's modulus, and Poisson's ratio equal to 560 kg/m^3, 1000 MPa, and 0.45, respectively. The soil plastic behavior was simulated using the Mohr–Coulomb model. The internal friction angle and the cohesion of the soil were set equal to 59.86° and 0.1 kPa, respectively, while the density of the soil Young's modulus and Poisson's ratio are equal to 2062 kg/m^3, 45 MPa, and 0.3, respectively. For validation with Tafreshi et al.'s [19] model, the internal friction angle and the density of the soil were set equal to 1972 kg/m^3 and 40.5°, respectively.

Indicative results of the validation are presented in Figure 2. According to the experimental data shown in Figure 2a, the level of the diameter changes rapidly increased from 0 to values higher than 6% after 25 loading cycles. In the sequence, the increase in the horizontal and vertical diameter changes decreased, reaching up to 7% and 8%, respectively, after 150 loading cycles [19]. The numerical model manages to capture the peak diameter change level accurately after 150 loading cycles. On the other hand, the numerical results present a slight discrepancy compared to the experimental data regarding the inclination of the curves, i.e., 50 cycles are needed in order to reach a 6% diameter change. Nevertheless, the obtained results confirm that the employed numerical approach is quite reliable in order to investigate the response of buried pipelines.

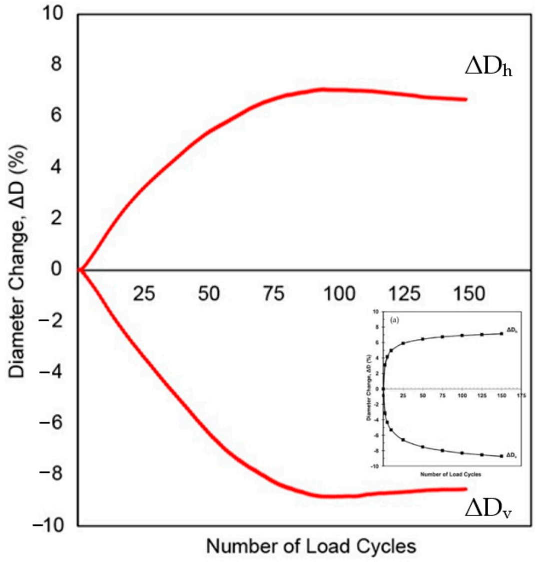

(**a**)

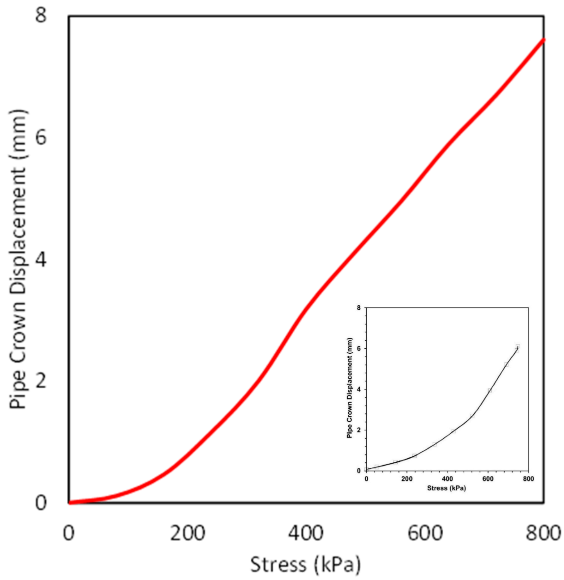

(**b**)

Figure 2. Validation with experimental data: (**a**) vertical (ΔD_v) and horizontal (ΔD_h) diametric change (comparison with results reused with permission from [19]); (**b**) pipe crown displacement (comparison with results taken from [24]).

This is further verified via validation with the second experimental test [24], in which the pipe crown displacement slightly increased from 0 to 2 mm when half of the total load was applied on the pipe. The increase in the pipe crown displacement increased more rapidly from 2 mm to 6 mm when the total load was applied to the model, as presented in Figure 2b. The numerical model slightly overestimates the pipe crown displacements compared to the experimental ones. Nonetheless, the shape of the curve is well captured, while the numerical values are very close to the experimental results. Hence, based on this successful validation (with the only available experimental data with buried pipes, EPS, and vehicle moving loads), it is verified that this computational approach could be extended to realistically and reliably simulate the more complex problem that is examined in this study.

2.2. Description of the HST Moving Loads and Buried Pipeline Numerical Model

In the sequence, the dynamic response of a steel pipeline located under an HSR line has been thoroughly investigated numerically by properly modifying the validated computational approach in order to implement the HST passing loads [26]. For this purpose, an advanced 3D numerical model consisting of finite elements and infinite elements was developed in order to simulate the problem at hand. In addition, the geometry and loads of a popular HST in Europe, i.e., Thalys train, were used. The steel pipeline was embedded to cross vertically at a shallow depth under the HSR track, as depicted in the sketch of Figure 3. Figure 4 presents the finite/infinite element model that has been developed. Due to the symmetry of the examined track along its longitude axis, only a part of the domain has been analyzed, as shown in Figure 4. The passage of the Thalys HST was implemented by imposing on the railway track multiple moving loads. For this purpose, a user-developed Vdload subroutine was used to input the multiple HST loads into the ABAQUS numerical model.

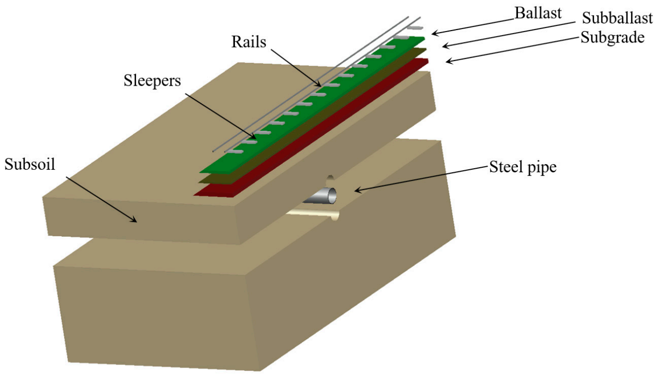

Figure 3. Sketch showing the track components, the soil, and the steel pipe.

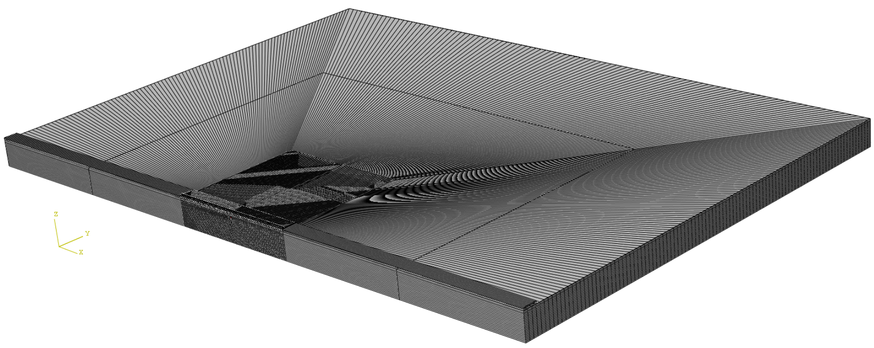

Figure 4. Numerical model: finite elements at the central part and surrounding infinite elements.

A typical at-grade European HSR configuration has been used for the conducted simulations [5]. This standard three-layered subgrade and foundation system consists of ballast, sub-ballast, and subgrade components based on the surrounding soil. Table 1 presents the mechanical properties of the track components. The mechanical properties of the single-layered soft clay subsoil are as follows: unit weight γ = 18 kN/m^3, Young's modulus E = 40 MPa, Poisson's ratio ν = 0.3, friction angle φ = 30°, and cohesion c = 10 kPa. The surrounding soil and all track components, except for the rail, have been simulated using 8-noded solid elements. In order to ensure the accuracy of the numerical simulations, the size of the finite elements was chosen to be equal to 20 cm. On the other hand, linear beam elements with 10 cm length were used for the simulation of the rail. The central part of the subsoil model has a total length equal to 50 m and is discretized via finite elements. Moreover, the subsoil layer has a depth of 30 m and a width of 50 m, as shown in Figure 4, and it is surrounded by infinite elements, aiming to prevent wave reflections along the edges of the FE model.

Table 1. Mechanical properties of track components.

Track Components	Layer Thickness (m)	Young's Modulus (GPa)	Poisson's Ratio (-)	Unit Weight (kN/m^3)
Rail	-	210	0.25	79
Sleepers	-	30	0.40	24
Ballast	0.3	0.1	0.35	18
Sub-ballast	0.2	0.3	0.35	22
Subgrade	0.5	0.127	0.35	21

HST moving loads quasi-static simulation was performed as time-depending stationary forces at the rail nodes. Each axle load (f_i) is constant, and its position was calculated at each time step (t) via its initial position (x_0) and the HST passing velocity (V_O). In the present investigation, three passing velocities are examined: quite low (240 km/h), typical operational (300 km/h), and high (360 km/h) velocities. At any time step in which the position of any axle load coincides with the position of a rail node, the whole axle force is considered to act on this node. On the other hand, at time steps in which the position of the moving load is acting on the span between two rail nodes, the moving load is divided into two parts acting on the two nodes of this rail span. According to this process, a user-developed subroutine was created in Fortran77 in order to incorporate train moving loads into the FE model. As previously mentioned, a commonly used train in central Europe, the Thalys HST, has been modeled in the present investigation. The total length of the Thalys HST is close to 200 m and consists of 26 axles and 10 bogies. Thalys bogies are categorized into three types: Y230A locomotive bogies and Y237A and Y237B passenger bogies. Figure 5 illustrates the geometry of the Thalys HST and its axle loads, with data taken from Kouroussis et al. [27].

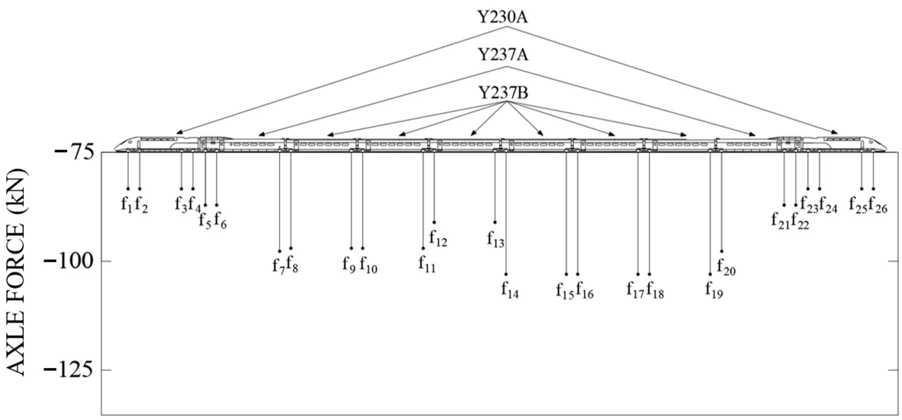

Figure 5. Thalys HST axle loads.

Initially, a commonly used transferring natural gas steel pipeline was examined; it has an outside diameter and thickness equal to 914 mm and 12.7 mm, respectively. The properties of X-65 steel material are as follows: tensile yield stress and ultimate strength 450 MPa and 560 MPa, while Young's modulus is 210 GPa. Figure 6a depicts the 3D sketch of the pipeline, while Figure 6b illustrates the corresponding mesh for the soil/track part and the embedded pipe. The burial depth of the pipeline was chosen to be equal to double the pipe's diameter, as is usually done in practice [28]. Furthermore, "hard contact" conditions have been selected for the interface, which allows for the separation of the pipeline from the subsoil, while the soil–pipeline interface friction parameter has been assumed to be equal to μ = 0.3 since this value is commonly used in relevant investigations [29,30].

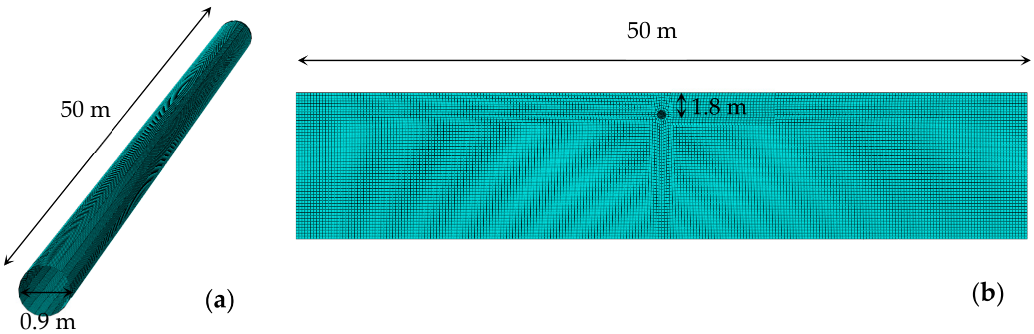

Figure 6. Finite-element discretization of the: (**a**) steel pipe; (**b**) pipe and soil cross-section.

Figure 7 presents the examined mitigation measure using a limited number of EPS blocks above the pipe. This approach is based on the so-called "imperfect trench method", which was proposed by the Norwegian Public Roads Administration (NPRA) [31,32]. According to the NPRA, a horizontal EPS-filled trench, with a 1.5D width, is placed at 0.2D above the pipe, where D is the diameter of the pipe. Herein, the examined steel pipe diameter is equal to 914 mm; thus, the EPS layer width and the distance from the pipe were set equal to 1371 mm and 182.8 mm, respectively. The recommended height of the EPS block according to the NPRA is equal to 50 cm. In the present investigation, the effectiveness of the EPS layer with several thicknesses between 12.5 cm and 50 cm has been examined in order to achieve an optimal balance between efficiency and cost.

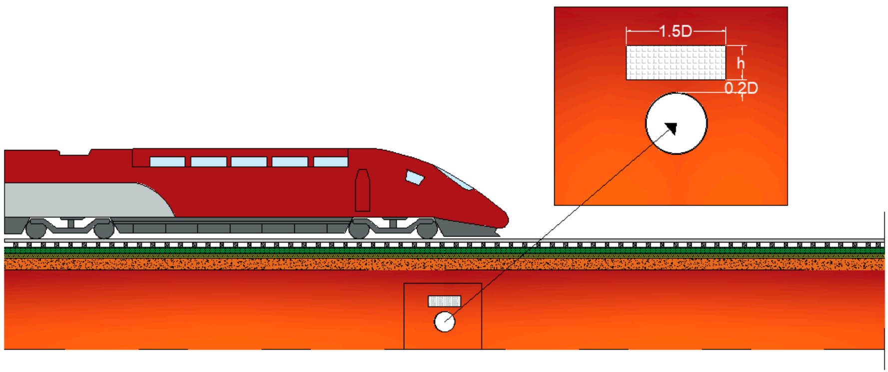

Figure 7. Recommended EPS layout above the pipe using the imperfect trench method.

As mentioned in the Introduction, EPS geofoam is a commonly used material in geotechnical applications; hence, there are various EPS materials with wide-ranging mechanical properties. According to ASTM D6817 [33], EPS geofoam is classified into seven categories (EPS12, EPS15, EPS19, EPS22, EPS29, EPS39, and EPS46). In the present study, EPS19, a relatively low-density geofoam, was selected as the trench fill material, with a Young modulus and Poisson's ratio of 4000 kPa and 0.05, respectively, whereas material damping is equal to 2%.

3. Results

3.1. Unprotected Pipeline Response

Initially, the dynamic response of the buried pipeline without the EPS protection layer was examined for three typical HST passage velocities: a relatively low velocity for HST (240 km/h), the typical Thalys operational velocity (300 m/s), and a quite high velocity (360 km/h). Figure 8 illustrates the Fourier spectra on the top of the pipeline for the examined passing velocities. In the sequence, the peak frequencies of each spectrum are derived via the Dominant Frequency Method (DFM) [34]. According to the DFM, the Fourier spectrum is strongly dependent on the train's velocity and the geometry of its bogies. Hence, these parameters are responsible for the most dominant vibration peaks. The dominant frequencies for which these peaks occur in the Fourier spectrum are well known as bogie passing frequencies ($f_{b,n}$). Furthermore, apart from $f_{b,n}$, there are two other dominant frequencies: the axle passing frequency (f_a), which depends on the distance of the HST's axles, and the sleeper passing frequency (f_s), which depends on the length of the sleeper's bay. The dominant passing frequencies of the bogies, the axles, and the sleepers can be calculated as follows:

$$f_{b,n} = n\frac{V_O}{l_b} \tag{1}$$

$$f_a = \frac{V_O}{l_a} \tag{2}$$

$$f_s = \frac{V_O}{l_s} \tag{3}$$

where l_b: bogie distance (18.7 m); l_a: bogie axles distance (18.7 m); l_s: sleeper bay; n = 1, 2, 3, . . .; and V_O: train passing velocity.

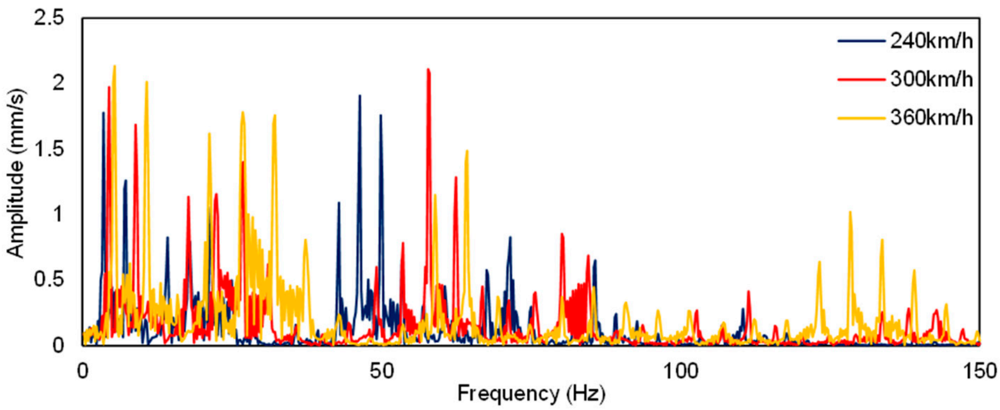

Figure 8. Fourier spectra at the unprotected pipeline top for HST passage with 240 km/h, 300 km/h, and 360 km/h.

The dominant frequencies are summarized in Table 2 for the three examined HST velocities. As illustrated in Figure 8, these frequencies are well captured in the results, which further verifies the validity of the developed numerical approach. In particular, the first six bogie passing frequencies have been captured quite accurately by the numerical model. The dominant peaks are placed at higher frequencies as the HST velocity increases from 240 km/h to 360 km/h. In the case of HST passing with low velocity (240 km/h), the most dominant frequencies are 3.5 Hz ($f_{b,1}$), 7.2 Hz ($f_{b,2}$), 46.4 Hz ($f_{b,13}$), and 49.9 Hz ($f_{b,14}$), and the vibration peaks vary between 1.3 mm/s and 2 mm/s. The peak at the axle passing frequency, close to 20 Hz, is also dominant and greater than 1 mm/s. In addition, the peak at the sleeper passing frequency has also been captured by the model, although it is quite low (3 mm/s).

Table 2. Dominant frequencies for the examined HST velocities.

Velocity (km/h)	$f_{b,1}$ (Hz)	$f_{b,2}$ (Hz)	$f_{b,3}$ (Hz)	$f_{b,4}$ (Hz)	$f_{b,5}$ (Hz)	f_a (Hz)	f_s (Hz)
240	4	7	11	14	18	20	111
300	4	9	13	18	22	25	139
360	5	11	16	21	27	30	167

The same observations can be derived when the Thalys train is running with its usual operational velocity (300 km/h). As expected, all the dominant peaks have been slightly moved to the right in this case. The first, the second, and the thirteenth passing frequencies of the bogies are the most dominant in the frequency range. These peaks are significantly increased compared to the passage with 240 km/h. For instance, the peak at $f_{b,1}$ has increased from 18 mm/s to 20 mm/s. The peaks at axle and sleeper passing frequencies are also slightly increased. For the highest passing velocity (360 km/h), except for the same dominant frequencies at lower velocities, several dominant peaks at other frequencies can be noticed. More specifically, at $f_{b,1}$ (5.4 Hz) and $f_{b,2}$ (10.7 Hz), the amplitude of the peaks is almost double, compared to the same values, in the case of Thalys' slower passage with 240 km/h. Nonetheless, it should be mentioned that the sleeper passing frequency has not been captured as it is quite high in this case (over 150 Hz).

3.2. Impact of EPS Layer Thickness on Pipeline Protection

Case 1: EPS layer with 12.5 cm height

In the first scenario, an EPS layer with a 12.5 cm thickness is implemented above the buried pipeline to reduce HST-induced vibrations. Figure 9a compares the Fourier spectra on the pipeline top before and after the implementation of the EPS blocks in the scenario of HST passage with 240 km/h. The beneficial role of the EPS layer is clearly illustrated, as all the dominant vibration peaks from 0 Hz to 100 Hz have been significantly reduced. For instance, the most dominant peak at 46.4 Hz has been reduced from 1.9 mm/s to 1.2 mm/s. Furthermore, the peaks at other dominant frequencies (e.g., 3.5 Hz, 7.2 Hz, 49.9 Hz) have a reduction equal to 40%. In the sequence, the effectiveness of the examined EPS layers has been investigated at the passage of Thalys with its typical operational velocity, 300 km/h.

As presented in Figure 9b, the high level of vibration peaks reduction is more evident in the lower frequency range (0~30 Hz). The proposed mitigation measure also plays a beneficial role at higher frequencies (>75 Hz). On the other hand, the examined mitigation measure is not effective at medium frequencies between 30 Hz and 75 Hz. Within this range, the most dominant frequency is located at 58 Hz, for which the EPS implementation slightly reduces the peak from 2.1 mm/s to 2 mm/s. Lastly, as shown in Figure 9c, the same trend is evident for the high passing velocity modeling scenario (360 km/h). A high reduction in all the vibration peaks at the low- and high-frequency range can also be observed. In this case, the most dominant frequencies are located at low frequencies (e.g., 5.4 Hz, 10.7 Hz, 26.5 Hz, 31.9 Hz), and the peaks of those frequencies have a reduction of over 40% compared to the unprotected pipe.

Case 2: EPS layer with 25 cm height

According to the previous results, the implementation of EPS blocks between the track and the buried pipeline successfully reduces HST-induced vibrations. Nevertheless, since the reduction in the vibrations level is relatively low, the implementation of a thicker layer of EPS is investigated in this section. More specifically, the thickness has been doubled; thus, the impact of an EPS layer with a thickness of 25 cm has been examined. As was expected, the vibration peaks remain at the same frequencies as previously, while the amplitude of the vibrations is substantially lower. For instance, in the case of an HST running with 240 km/h, the dominant peak at 46 Hz is reduced to 0.8 mm/s, 50% lower than 1.2 mm/s the layer with a height of 12.5 cm (see Figure 10a). The same observation can be made for all dominant frequencies, with amplitude reduction of up to 50%. Figure 10b illustrates the Fourier spectra for HST passage with 300 km/h. The peak vibrations level is reduced to 1.5 mm/s at 58 Hz. Furthermore, it should be mentioned that all the other vibration peaks are kept under 1 mm/s. The reduction in the vibrations level is also remarkable when the HST runs at high velocity (360 km/h) as all vibration peaks have been successfully reduced under 1 mm/s (see Figure 10c). It should be mentioned that vibration peaks at the high-frequency range are almost zero after implementing EPS blocks with 25 cm height.

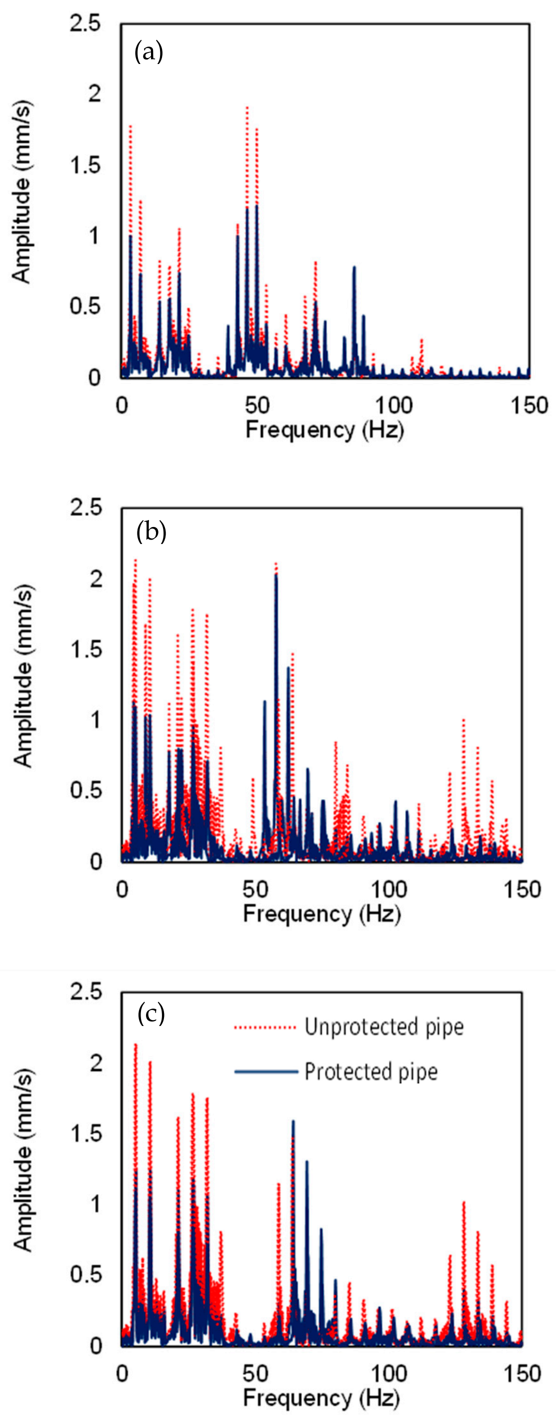

Figure 9. Fourier spectra at the pipeline top when protected with 12.5 cm thickness EPS layer for HST passage with (**a**) 240 km/h, (**b**) 300 km/h, and (**c**) 360 km/h.

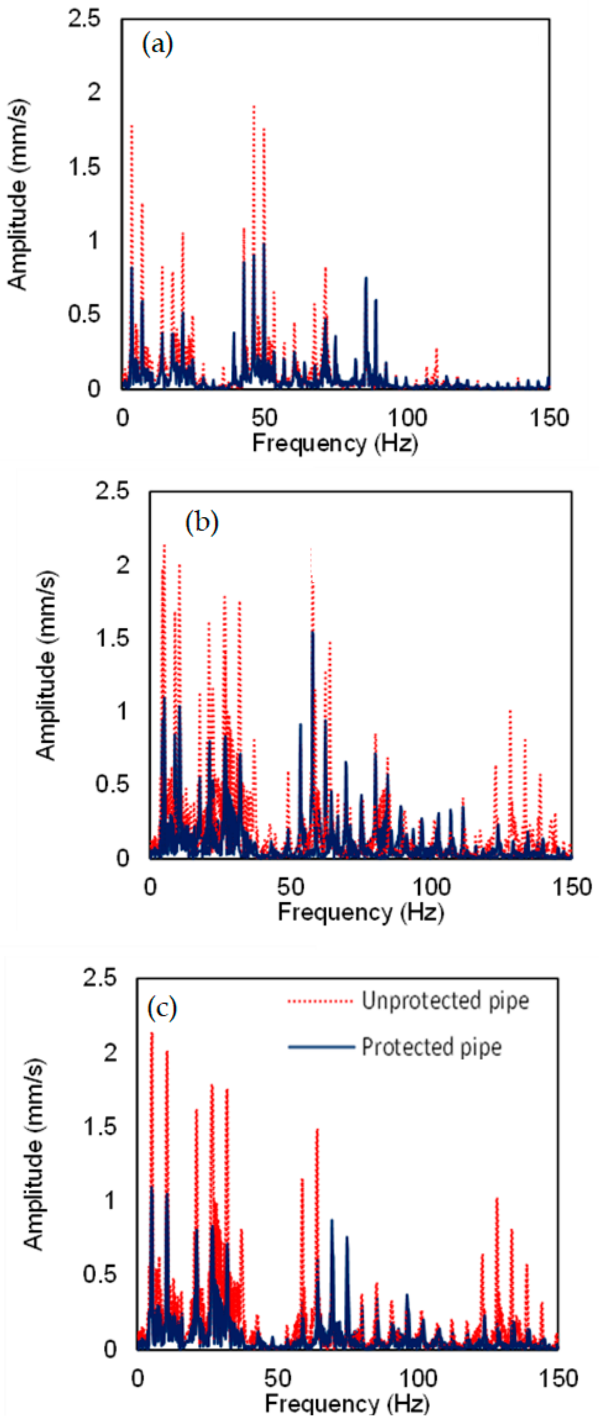

Figure 10. Fourier spectra at the pipeline top when protected with 25 cm thickness EPS layer for HST passage with (**a**) 240 km/h, (**b**) 300 km/h, and (**c**) 360 km/h.

Case 3: EPS layer with 50 cm height

The height of the EPS layer has been increased to 50 cm, aiming to further reduce the vibration levels. Figure 11 depicts the Fourier spectra for this mitigation measure. Evidently, the thicker EPS layer effectively reduces HST-induced vibrations for all the examined velocities. For low HST-passing velocity, the vibration peaks have been limited under 0.8 mm/s (see Figure 11a). Similarly, as shown in Figure 11b, in the case of the typical operation velocity of Thalys (300 km/h), the reduction reaches over 60% for certain frequencies (e.g., $f_{b,1}$, $f_{b,2}$). Lastly, the effectiveness of the examined mitigation measure is also significant for the highest examined passing velocity, as illustrated in Figure 11c. For instance, the vibration peaks at the most dominant frequencies ($f_{b,1}$, $f_{b,2}$) have been reduced from 2.2 mm/s and 2 mm/s to 0.8 mm/s and 0.9 mm/s, respectively.

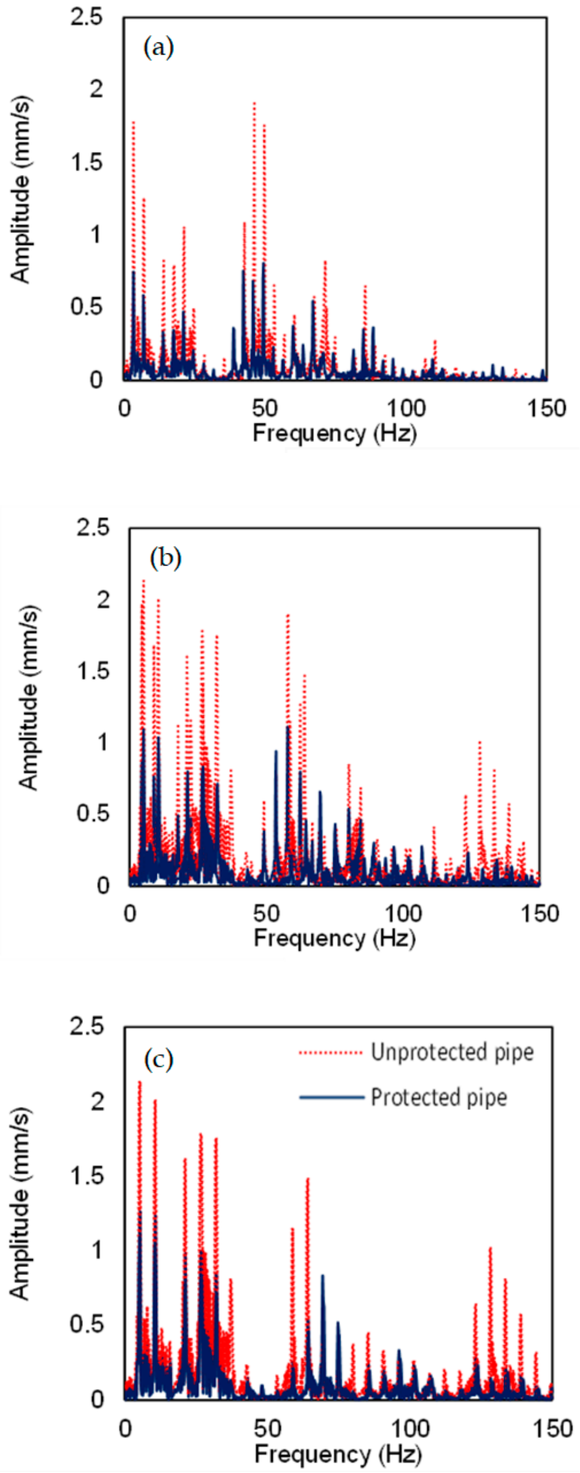

Figure 11. Fourier spectra at the pipeline top when protected with 50 cm thickness EPS layer for HST passage with (**a**) 240 km/h, (**b**) 300 km/h, and (**c**) 360 km/h.

Comparison of Performance Indices

In the sequence, the efficiency of the examined mitigation measure for each HST passing velocity is presented in terms of insertion loss (*IL*) curves [35,36]. The *IL* levels have been calculated for the center frequencies of the 1/3 octave bands between 1.25 Hz and 40 Hz according to the following expression [37]:

$$IL = 20\ log_{10} \frac{V_{rms,soil}}{V_{rms,mit}} \tag{4}$$

where $V_{rms,soil}$: soil cutting root mean square of the spectral velocity at each center frequency; $V_{rms,mit}$: mitigated cutting root mean square of the spectral velocity at each center frequency.

Figure 12 demonstrates the insertion loss (*IL*) of the examined mitigation measure in the three cases of HST velocities. *IL* has been computed at the center frequency of each one-third octave band, from 1.25 to 125 Hz, and the results were averaged to one-third octave bands. In the case of the implementation of an EPS-filled trench with 12.5 cm height, the *IL* remains at the same level for all the examined velocities in all octave bands with central frequencies lower than 31.5 Hz. More specifically, the insertion loss is close to 4.8 dB for these middle octave bands. At the higher octave bands, the insertion loss varies between extremely low or high values. In general, the use of an EPS layer with a 12.5 cm thickness slightly reduces the vibrations level at the top of the pipeline, yet this reduction is not satisfactory.

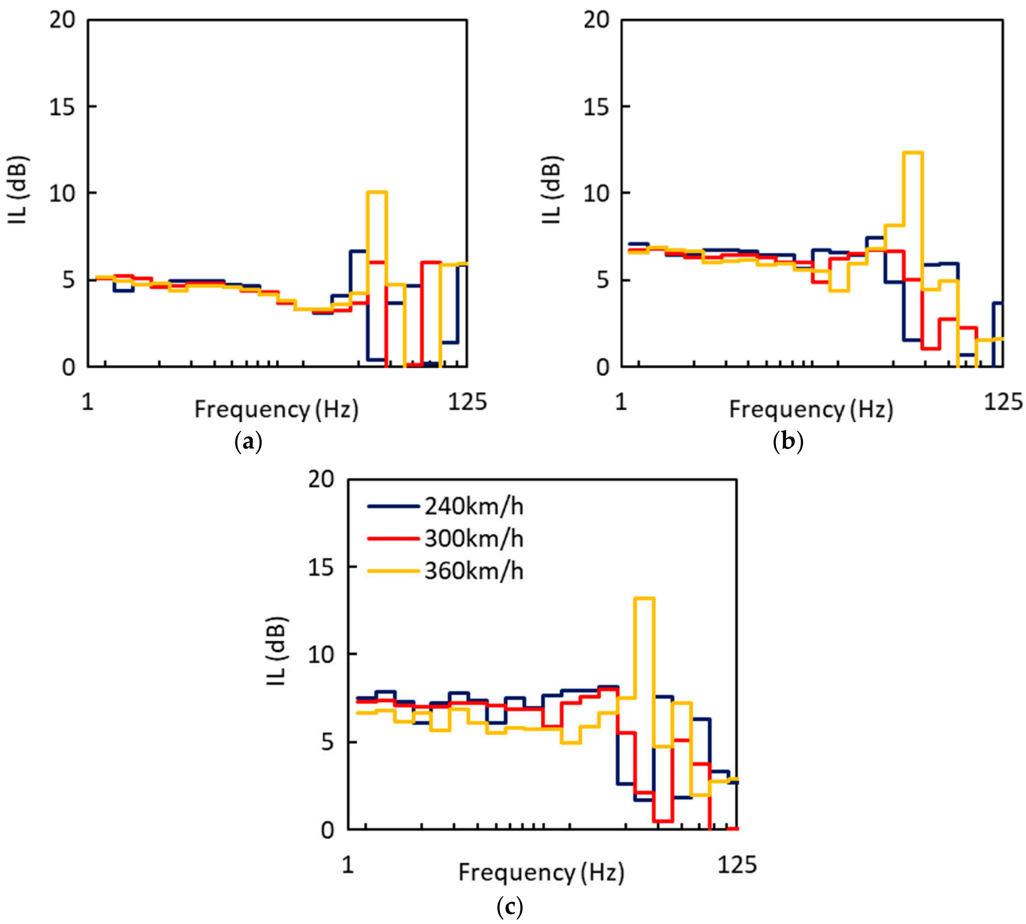

Figure 12. Insertion loss curves at the pipeline top for EPS layer with thickness equal to (**a**) 12.5 cm (**b**) 25 cm, and (**c**) 50 cm.

Figure 12b illustrates the *IL* curves for the 25 cm EPS layer, where the insertion loss is increased compared to the previous case. Herein, the amplitude of insertion loss at the octave bands with a center frequency below 31.5 Hz is close to 6.7 dB for all the examined HST passing velocities. The insertion loss reaches its peak value of 12 dB at the 1/3 octave band with a center frequency of 40 Hz after implementing EPS19 when Thalys passes with

360 km/h. Figure 12c shows the insertion loss curve for the thicker EPS layer of the present investigation. The insertion loss is increased in comparison with the cases of thinner EPS layers, i.e., *IL* ranges close to 7.3 dB for the octave bands with center frequencies lower than 31.5 Hz. Those values remain at the same level for all the examined frequencies. It should be mentioned that the insertion loss also varies for the higher 1/3 octave bands.

In addition, a commonly used vibration index, i.e., the peak particle velocity (*PPV*), has been used to assess the efficiency of each EPS configuration. DIN 4150-3 standard defines the *PPV* as follows [38]:

$$PPV = \max\left|\sqrt{v_x^2(\mathrm{t}) + v_y^2(\mathrm{t}) + v_z^2(t)}\right| \quad (5)$$

where v_x(t), v_y(t), and v_z(t) are the longitudinal, transversal, and vertical velocity time-histories, respectively. As it is clearly illustrated in Figure 13, the most effective mitigation measure is the implementation of a thick layer (50 cm) with low-density EPS19 blocks. As the HST passing velocity increases, the *PPV* level is also increased. The same trend is observed for the thinner EPS19 layers.

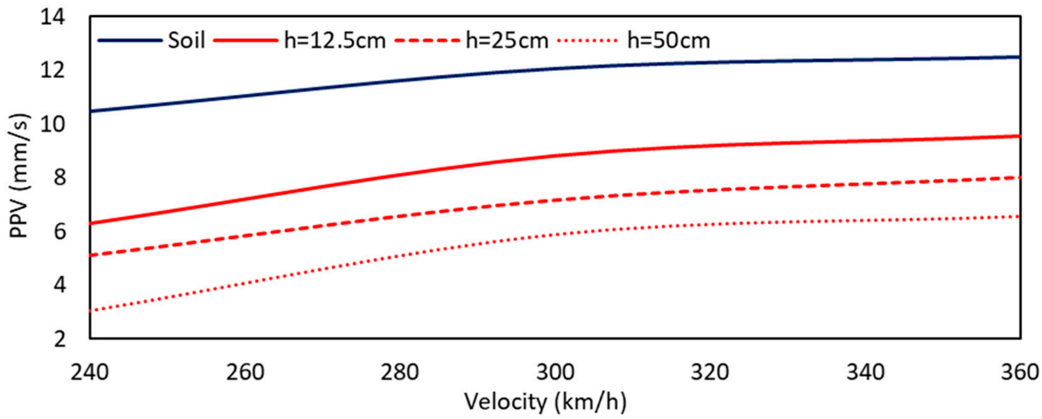

Figure 13. Relationship between *PPV* levels at the pipeline top and the increasing passing velocity for various EPS layer heights.

Figure 14 depicts the *PPV* levels at the top of the pipeline at an increasing distance from the HST passing axis. As was expected, the *PPV* values are (slightly) reduced at an increasing distance from the track both for the protected and the unprotected pipeline. Evidently, the *PPV* on the top of the pipeline is reduced rapidly for all the examined passing velocities when the EPS layer with a height of 50 cm is added for all EPS heights. For example, when the Thalys HST is passing with 240 km/h, the *PPV* of the unprotected pipeline is reduced from 3.7 mm/s to 1.4 mm/s at 6 m from the track. The corresponding values after the implementation of EPS19 were decreased to 2.6 mm/s and 1.4 mm/s (at 6 m). The same tends were noticed for an HST passing with 300 km/h and 360 km/h. Lastly, it is also obvious that the proposed mitigation measure does not affect the vibrations level at distances higher than 6 m from the rail axis.

3.3. Impact of Pipeline Material and Geometry

Previous results have clearly presented the beneficial role of the implementation of EPS geofoam in the reduction in vibration levels on the pipe surface. This reduction can significantly reduce damage probability during the life-cycle of such important infrastructure, which is even more crucial in the case of gas pipelines. Apart from the induced vibrations, it is important to investigate the effect of the HST dynamic loads on the distress of the pipeline in terms of its potential ovalization, i.e., diameter change. As mentioned, the level of the diameter change is crucial for the integrity and safe operation of the pipelines. The pipeline examined in the previous section is quite thick and stiff (e.g., 12.7 mm); hence, its diameter change is marginal, as illustrated in Figure 15. It is evident that the vertical diameter change in the unprotected pipeline is equal to 0.3 mm at the passage of each HST bogie (see Figure 15a). This value is reduced below 0.2 mm after the implementation of an EPS19 layer with a thickness of 50 mm. As presented in Figure 15b, the same observation can be made regarding the horizontal diameter change. Furthermore, the vertical and horizontal residual deformations after HST passage are almost zero. For this reason, it can be assumed that the shape of the pipe is not altered regardless of the EPS application.

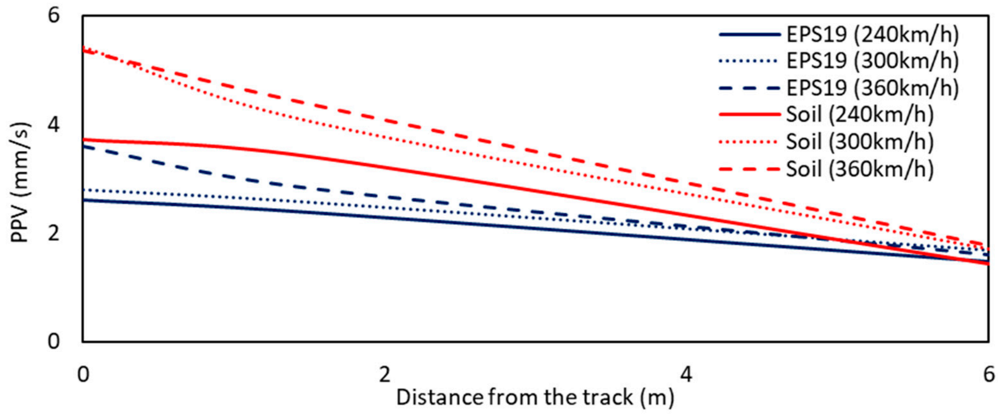

Figure 14. Relationship between *PPV* levels at the pipeline top and the increasing distance from the rail axis.

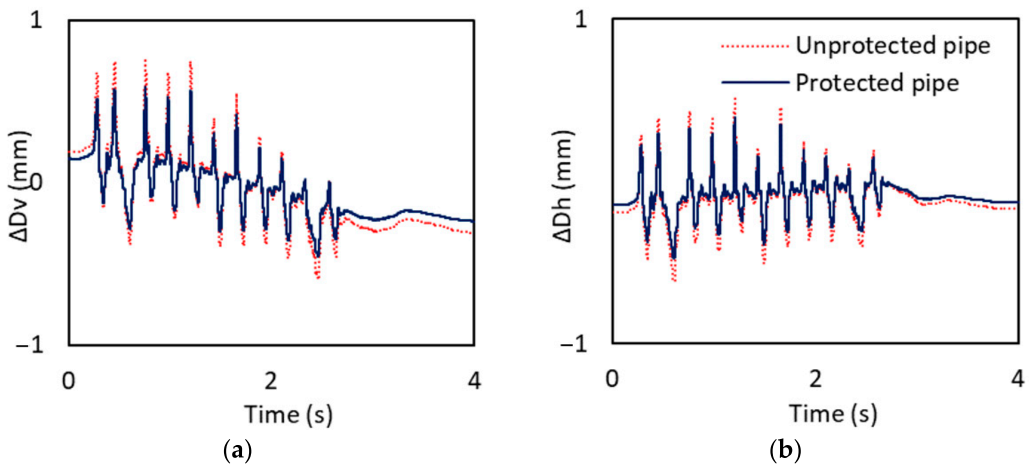

Figure 15. Impact of EPS on large steel pipe (with diameter D = 914 mm) diameter change: (**a**) vertical and (**b**) horizontal directions.

Nevertheless, pipelines with a lower thickness, other material, and and/or smaller burial depths are more prone to significant deformations. For this reason, a HDPE100 (i.e., from the same material that has been used for the initial validation in Section 2.1) pipe with a diameter of 250 mm and thickness of 3 mm has been placed at a 0.5 m depth under the HSR line to investigate its deformations due to the passage of HST Thalys, as has been previously presented for the steel pipe. Analogously, the HDPE100 pipeline has also been protected with a 25 cm EPS layer. In order to investigate the effect of pipe thickness on the response of the HDPE100 pipeline, a similar pipe with an increased thickness (9 mm) has also been examined.

Figure 16 displays the impact of HST passage on the diameter change in the polyethylene pipelines with the same diameter and thickness equal to 3 mm or 9 mm. As expected, the diameter change in the pipeline is significantly higher compared to the previously examined larger and stiffer steel pipe. At the first HST axle passage, the vertical diameter change in the unprotected pipe with 3 mm thickness is equal to 1.6 mm. The deformation gradually increased, reaching the maximum value of 7 mm at the passage of the last boogie.

Furthermore, the peak deformation oscillation width is close to 6 mm, while a vertical residual deflection equal to 0.8 mm is observed after HST passage. Evidently, the EPS layer has a beneficial impact on the reduction in the pipe diameter change, as it has reduced the peak vertical deformation from 7 mm to 3 mm, while the oscillation width is drastically minimized to 1 mm. As shown in Figure 16b, similar observations for the effectiveness of the EPS mitigation measure can be made for the horizontal diameter change. The horizontal residual deformation is significantly higher than the vertical, exceeding 2 mm for the unprotected pipe, whereas the application of the EPS layer reduces it to approximately 1 mm.

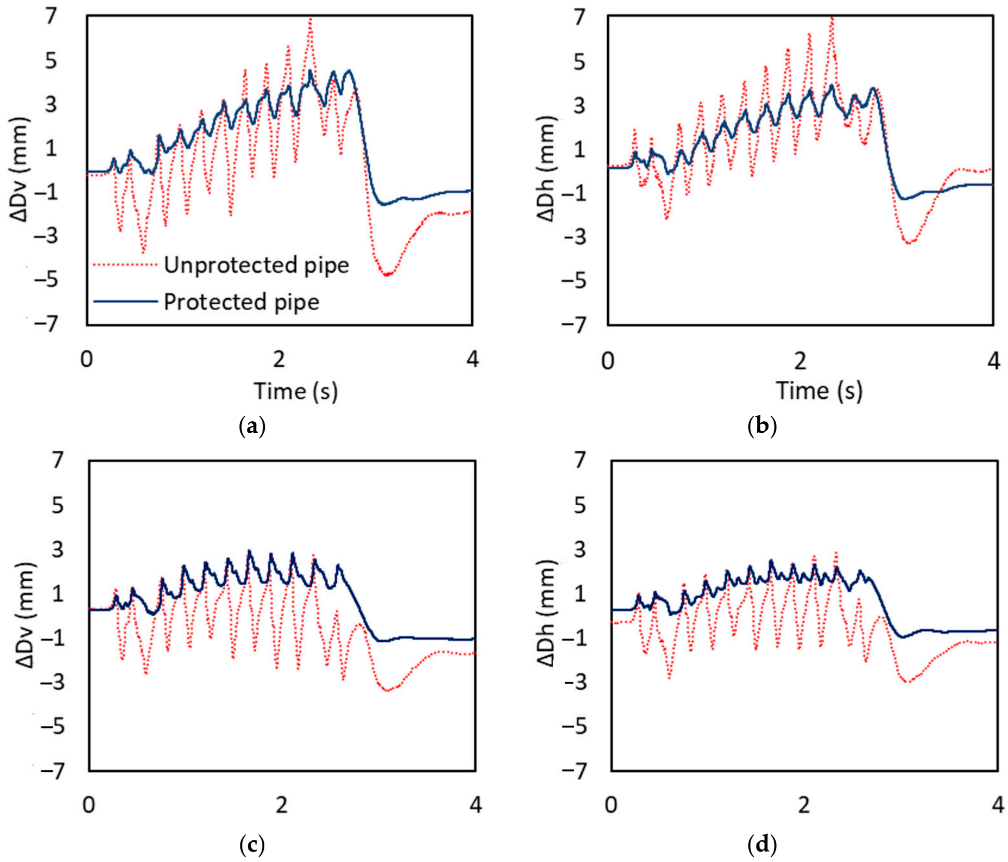

Figure 16. (**a**) Vertical and (**b**) horizontal diameter change for a polyethylene pipe with D = 250 mm for thickness equal to 3 mm; (**c**) vertical and (**d**) horizontal diameter change for thickness equal to 9 mm.

Figure 16c,d compare the response of a thicker polyethylene pipe before and after adding the EPS layer. As expected, the increase in the pipeline thickness reduces the pipe vertical and horizontal deformations to below 3 mm, whereas the residual deformation at both directions is equal to 1.3 mm. Nevertheless, the oscillation width remains high (equal to 5 mm and 5.5 mm for the vertical and horizontal deformations, respectively). The beneficial role of the EPS layer is also obvious in this case. Especially in the vertical dimension, where the peak oscillation width has been reduced to below 0.4 mm and the residual deformation is less than 1 mm.

In the sequence, two smaller steel pipelines made also from X-65 material and with a diameter equal to 250 mm and thicknesses of 3 mm and 9 mm have also been studied. The diameter change in the smaller steel pipes is presented in Figure 17. The peak deformation of the unprotected steel pipe with a 3 mm thickness is equal to 3 mm and 2.8 mm at the vertical and horizontal directions, as shown in Figure 17a,b. The horizontal and vertical residual deformations are equal to 0.8 mm and 0.2 mm, while the oscillation width is equal to 3 mm. Obviously, the steel pipe is substantially more resistant to HST-induced vibrations compared to the polyethylene pipe with the same geometry. Nonetheless, it is evident that the examined protection scheme significantly reduces HST-induced deformations. More specifically, the vertical residual deformation is reduced to almost zero, whereas the horizontal residual deformation is decreased from 0.8 mm to 0.2 mm, as illustrated in Figure 17b. On the other hand, the impact of HST passage on the thicker steel pipe is marginal. More specifically, the vertical peak deformation remains below 0.3 mm for a pipe with a 9 mm thickness (see Figure 17c). As illustrated in Figure 17d, the same trend occurs along the horizontal direction, in which the diameter change is marginal, and the residual deformation is almost zero after the implementation of the EPS layer.

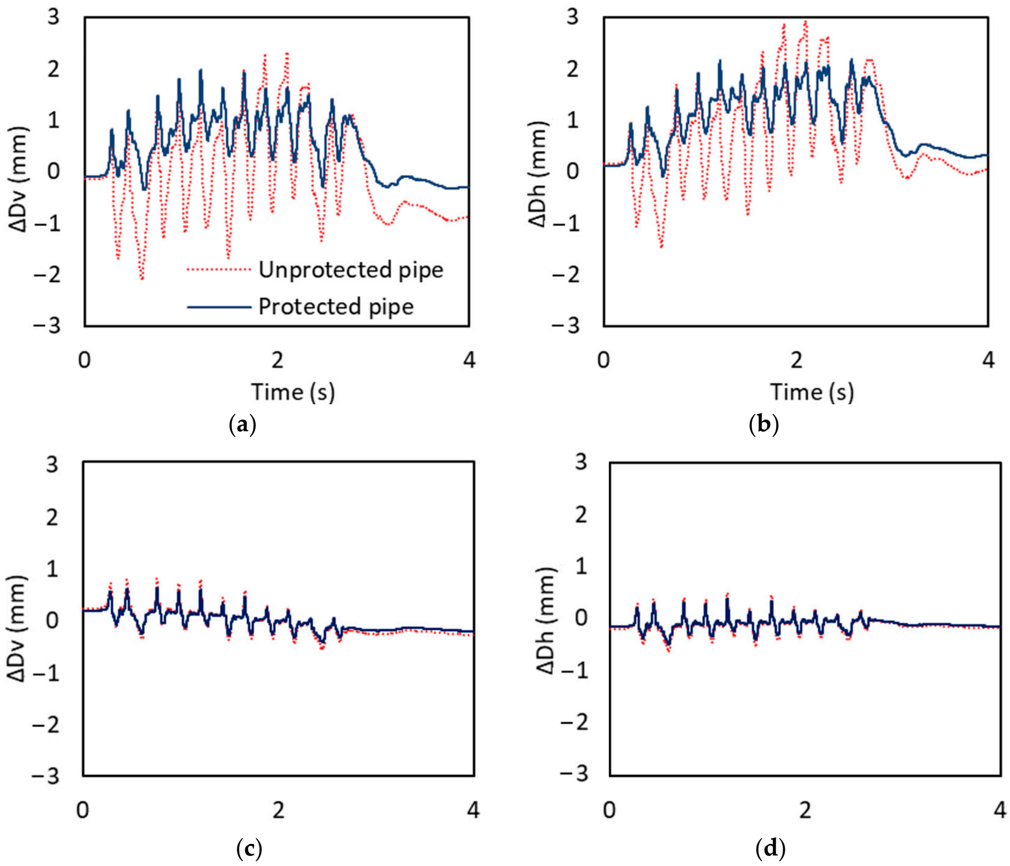

Figure 17. (**a**) Vertical and (**b**) horizontal diameter change for a steel pipe with $D = 250$ mm for thickness equal to 3 mm; and (**c**) vertical and (**d**) horizontal diameter change for thickness equal to 9 mm.

4. Discussion

In the present work, a cost-efficient mitigation measure utilizing EPS backfill for buried pipelines subjected to vibrations induced by HST passage has been examined. This problem was investigated by performing a numerical parametric study utilizing ABAQUS finite-element software. Regarding pipe response, the numerical model was partially validated with available experimental data regarding the use of EPS for buried pipe protection under traffic loads [19,23] due to a lack of available data for train moving loads. Nonetheless, the employed numerical methodology has been extensively validated in some authors' previous studies (e.g., [13,26]) with in situ measurements of HST passage without the presence of pipelines.

Low-density EPS19 was used as a backfill material above the pipe. Furthermore, the impact of the pipe material and geometry on its deformations and the diameter change has been investigated by comparing steel and polyethylene pipelines with varying dimensions. The implementation of this low-density backfill has contributed to reducing the vibrations level on the top of both steel and, especially, polyethylene pipelines. In order to examine the efficiency of the examined mitigation measure, the passage of Thalys HST with three different velocities has been investigated. To compare the results among the unprotected and protected pipes, commonly used indicators in the field of traffic-induced vibrations have been used, while the vertical and horizontal deformations, i.e., pipe ovalization, have also been compared.

The main findings of the present investigation could be summarized as follows:

- Implementing an EPS layer between the track and the buried pipeline substantially reduces HST-induced vibrations.
- The insertion loss at the center frequencies of the lower 1/3 octave bands is constant and independent from the HST passing velocity.
- The reduction in the vibrations level strongly depends on the thickness of the EPS layer.
- The material and dimensions of the pipe affect the results both for unprotected and protected cases. Thick steel pipes are less vulnerable; thus, the implementation of EPS may not be needed.
- The transient and residual deformations of polyethylene pipes are higher compared to those of steel pipes. Hence, the efficiency of the application of the EPS layer is more pronounced in this case.

5. Conclusions

The main contribution of the current study is that it presents the impact of HST-induced vibrations on buried pipelines vertically crossing under an HSR line. It has to be stressed that the continuous expansion of HSR in urban environments will increase the occurrences of crossings with various types of lifelines. Another novelty is that it highlights the beneficial role of the proposed mitigation scheme using EPS for the reduction in the distress of the pipelines. Several researchers have applied the examined mitigation measure, i.e., EPS blocks, in order to protect buried pipelines subjected to permanent ground displacements, yet they have not included HST moving loads and the consequent vibrations. The impact of the proposed mitigation measure on various types of pipes has been presented for varying dynamic loading conditions. The present investigation concludes that the implementation of the proposed mitigation measure could successfully protect the buried pipelines from such dynamic loads. Hence, the application of a thin EPS layer above any type of pipe constitutes an easily applicable and cost-efficient protection method.

The findings of this study will be useful for designing lifelines close to HSR lines and could be the basis for formulating practical guidelines. Nonetheless, since this is a first attempt to investigate the effectiveness of EPS between an HSR line and a buried pipe, further investigation is required to ensure the efficiency of the proposed mitigation measure. For instance, different soil conditions, train geometry, and loads that affect the frequency content of the vibrations, material non-linearities, EPS properties, and dimensions, issues related to the life-cycle performance of EPS, should also be examined in future extensions of the current work. Evidently, the effectiveness of the proposed mitigation measure would be further verified by performing a real-scale experiment.

Author Contributions: Conceptualization, A.L., Y.T. and P.N.P.; methodology, A.L., Y.T. and P.N.P.; software, A.L.; validation, A.L. and Y.T.; formal analysis, A.L., Y.T. and P.N.P.; investigation, A.L., Y.T. and P.N.P.; resources, A.L. and Y.T.; data curation, A.L., Y.T. and P.N.P.; writing—original draft preparation, A.L., Y.T. and P.N.P.; writing—review and editing, A.L., Y.T. and P.N.P.; visualization, A.L., Y.T. and P.N.P.; supervision, Y.T.; project administration, Y.T. All authors have read and agreed to the published version of the manuscript.

Funding: This research is co-financed by Greece and the European Union (European Social Fund-ESF) through the Operational Programme "Human Resources Development, Education and Lifelong Learning 2014–2020" in the context of the project "Strengthening Human Resources Research Potential via Doctorate Research—2nd Cycle" (MIS 5000432).

Institutional Review Board Statement: Not applicable.

Informed Consent Statement: Not applicable.

Data Availability Statement: The data presented in this study are available on request from the corresponding author. The data are not publicly available due to privacy reasons.

Conflicts of Interest: The authors declare no conflicts of interest. No funders had any role in the design of the study; in the collection, analyses, or interpretation of the data; in the writing of the manuscript; or in the decision to publish the results.

References

1. Connolly, D.P.; Marecki, G.P.; Kouroussis, G.; Thalassinakis, I.; Woodward, P.K. The growth of railway ground vibration problems—A review. *Sci. Total Environ.* **2016**, *568*, 1276–1282. [CrossRef]
2. Kuo, K.A.; Papadopoulos, M.; Lombaert, G.; Degrande, G. The coupling loss of a building subject to railway induced vibrations: Numerical modelling and experimental measurements. *J. Sound Vib.* **2019**, *442*, 459–481. [CrossRef]
3. López-Mendoza, D.; Connolly, D.P.; Romero, A.; Kouroussis, G.; Galvín, P. A transfer function method to predict building vibration and its application to railway defects. *Constr. Build. Mater.* **2020**, *232*, 117217. [CrossRef]
4. Yao, J.; Zhao, R.; Zhang, N.; Yang, D. Vibration isolation effect study of in-filled trench barriers to train-induced environmental vibrations. *Soil Dyn. Earthq. Eng.* **2019**, *125*, 105741. [CrossRef]
5. Kouroussis, G.; Verlinden, O.; Conti, C. Free field vibrations caused by high-speed lines: Measurement and time domain simulation. *Soil Dyn. Earthq. Eng.* **2011**, *31*, 692–707. [CrossRef]
6. Connolly, D.; Giannopoulos, A.; Forde, M.C. Numerical modelling of ground borne vibrations from high speed rail lines on embankments. *Soil Dyn. Earthq. Eng.* **2013**, *46*, 13–19. [CrossRef]
7. Beena, K.S.; Sandeep, M.N.; Indraratna, B.; Malisetty, R.S. Near-field vibrations in railway track on soft subgrades for semi high-speed trains. *Transp. Eng.* **2023**, *12*, 100176. [CrossRef]
8. Çelebi, E.; Kırtel, O. Non-linear 2-D FE modeling for prediction of screening performance of thin-walled trench barriers in mitigation of train-induced ground vibrations. *Constr. Build. Mater.* **2013**, *42*, 122–131. [CrossRef]
9. Gao, G.; Bi, J.; Chen, J. Vibration mitigation performance of embankments and cuttings in transversely isotropic ground under high-speed train loading. *Soil Dyn. Earthq. Eng.* **2020**, *141*, 106478. [CrossRef]
10. Sheng, X.; Jones, C.J.C.; Thompson, D.J. Prediction of ground vibration from trains using the wavenumber finite and boundary element methods. *J. Sound Vib.* **2006**, *293*, 575–586. [CrossRef]
11. Li, L.; Nimbalkar, S.; Zhong, R. Finite element model of ballasted railway with infinite boundaries considering effects of moving train loads and Rayleigh waves. *Soil Dyn. Earthq. Eng.* **2018**, *114*, 147–153. [CrossRef]
12. Gao, G.; Yao, S.; Yang, J.; Chen, J. Investigating ground vibration induced by moving train loads on unsaturated ground using 2.5D FEM. *Soil Dyn. Earthq. Eng.* **2019**, *124*, 72–85. [CrossRef]
13. Lyratzakis, A.; Tsompanakis, Y.; Psarropoulos, P.N. Mitigating high-speed train vibrations with EPS blocks for various soil conditions. *Soil Dyn. Earthq. Eng.* **2020**, *141*, 106482. [CrossRef]
14. Liolios, A.; Profillidis, V.; Christodoulidis, D.; Tantanozis, N. A Computational approach to the dynamic soil-pipeline interaction induced by high-speed railway traffic. In Proceedings of the 15th Nordic Seminar on Computational Mechanics, Aalborg, Denmark, 18–19 October 2002; pp. 259–262.
15. Puppala, A.J.; Ruttanaporamakul, P.; Congress, S.S.C. Design and construction of lightweight EPS geofoam embedded geomaterial embankment system for control of settlements. *Geotext. Geomembr.* **2019**, *47*, 295–305. [CrossRef]
16. Liyanapathirana, D.S.; Ekanayake, S.D. Application of EPS geofoam in attenuating ground vibrations during vibratory pile driving. *Geotext. Geomembranes* **2016**, *44*, 59–69. [CrossRef]
17. Alfheim, S.; Refsdal, G.; Rygg, N. The first EPS geoblock road embankment—1972. In Proceedings of the 4th International Conference on Geofoam Blocks in Construction Applications, Lillestrøm, Norway, 6–8 June 2011; pp. 1–10.
18. Bartlett, S.F.; Lingwall, B.N.; Vaslestad, J. Methods of protecting buried pipelines and culverts in transportation infrastructure using EPS geofoam. *Geotext. Geomembr.* **2015**, *43*, 450–461. [CrossRef]
19. Tafreshi, S.N.M.; Darabi, N.J.; Dawson, A.R. Geotextiles and Geomembranes Combining EPS geofoam with geocell to reduce buried pipe loads and trench surface rutting. *Geotext. Geomembranes* **2020**, *48*, 400–418. [CrossRef]
20. Choo, Y.W.; Abdoun, T.H.; O'Rourke, M.J.; Ha, D. Remediation for buried pipeline systems under permanent ground deformation. *Soil Dyn. Earthq. Eng.* **2007**, *27*, 1043–1055. [CrossRef]
21. Rasouli, H.; Fatahi, B. Geofoam blocks to protect buried pipelines subjected to strike-slip fault rupture. *Geotext. Geomembr.* **2020**, *48*, 257–274. [CrossRef]
22. Kim, H.; Choi, B.; Kim, J. Reduction of Earth Pressure on Buried Pipes by EPS Geofoam Inclusions. *Geotech. Test. J.* **2010**, *33*, 304–313. [CrossRef]
23. Witthoeft, A.F.; Kim, H. Numerical investigation of earth pressure reduction on buried pipes using EPS geofoam compressible inclusions. *Geosynth. Int.* **2016**, *23*, 287–300. [CrossRef]
24. Khalaj, O.; Azizian, M.; Darabi, N.J.; Tafreshi, S.N.M.; Jirková, H. The role of expanded polystyrene and geocell in enhancing the behavior of buried HDPE pipes under trench loading using numerical analyses. *Geosciences* **2020**, *10*, 251. [CrossRef]
25. *ABAQUS*, Analysis User's Manual Ver. 6.14; Dassault Systèmes Simulia Corp.: Providence, RI, USA, 2014.

26. Lyratzakis, A.; Tsompanakis, Y.; Psarropoulos, P.N. Efficient mitigation of high-speed trains induced vibrations of railway embankments using expanded polystyrene blocks. *Transp. Geotech.* **2020**, *22*, 100312. [CrossRef]
27. Kouroussis, G.; Verlinden, O. Prediction of railway ground vibrations: Accuracy of a coupled lumped mass model for representing the track/soil interaction. *Soil Dyn. Earthq. Eng.* **2015**, *69*, 220–226. [CrossRef]
28. Mohitpour, M.; Golshan, H.; Murray, A. *Pipeline Design & Construction: A Practical Approach*, 3rd ed.; ASME Press: New York, NY, USA, 2007. [CrossRef]
29. Demirci, H.E.; Bhattacharya, S.; Karamitros, D.; Alexander, N. Experimental and numerical modelling of buried pipelines crossing reverse faults. *Soil Dyn. Earthq. Eng.* **2018**, *114*, 198–214. [CrossRef]
30. Vazouras, P.; Karamanos, S.A.; Dakoulas, P. Finite element analysis of buried steel pipelines under strike-slip fault displacements. *Soil Dyn. Earthq. Eng.* **2010**, *30*, 1361–1376. [CrossRef]
31. NPRA. *Håndbok 016: Geoteknikkivegbygging*; Norwegian Public Roads Administration: Lillehammer, Norway, 2010. (In Norwegian)
32. Kang, J. Finite element analysis for deeply buried concrete pipes in proposed imperfect trench installations with expanded polystyrene (EPS) foams. *Eng. Struct.* **2019**, *189*, 286–295. [CrossRef]
33. *ASTM D6817*; Standard Specification for Rigid Cellular Polystyrene Geofoam. ASTM: West Conshohocken, PA, USA, 2017. Available online: www.astm.org (accessed on 10 June 2022).
34. Kouroussis, G.; Connolly, D.P.; Forde, M.C.; Verlinden, O. Train speed calculation using ground vibrations. *Proc. Inst. Mech. Eng. Part F J. Rail Rapid Transit* **2013**, *229*, 466–483. [CrossRef]
35. Li, T.; Su, Q.; Kaewunruen, S. Seismic metamaterial barriers for ground vibration mitigation in railways considering the train-track-soil dynamic interactions. *Constr. Build. Mater.* **2020**, *260*, 119936. [CrossRef]
36. Ngamkhanong, C.; Kaewunruen, S. Effects of under sleeper pads on dynamic responses of railway prestressed concrete sleepers subjected to high intensity impact loads. *Eng. Struct.* **2020**, *214*, 110604. [CrossRef]
37. Coulier, P.; Dijckmans, A.; Jiang, J.; Thompson, D.; Degrande, G.; Lombaert, G. Stiff wave barriers for the mitigation of railway induced vibrations. In Proceedings of the 11th International Workshop on Railway Noise, Uddevalla, Sweden, 9–13 September 2013. [CrossRef]
38. *DIN 4150-3*; Structural Vibrations—Part 3: Effects of Vibration on Structures. DIN Germany Institute: Berlin, Germany, 1999.

Disclaimer/Publisher's Note: The statements, opinions and data contained in all publications are solely those of the individual author(s) and contributor(s) and not of MDPI and/or the editor(s). MDPI and/or the editor(s) disclaim responsibility for any injury to people or property resulting from any ideas, methods, instructions or products referred to in the content.